Heliyon 10 (2024) e37540

Contents lists available at ScienceDirect

Heliyon

journal homepage: www.cell.com/heliyon

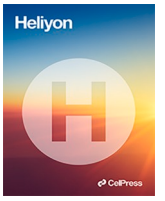

Research article

Synthesis, characterization of hydroxyapatite from pomegranate fruit peel for Cr (VI) adsorption: Process modelling, kinetic and isotherm studies

Suman Pawar [a], Thomas Theodore [b,*]

[a] Department of Chemical Engineering, Siddaganga Institute of Technology, Tumakuru, India
[b] School of Chemical Engineering, Vellore Institute of Technology, Vellore, Tamil Nadu, India

ARTICLE INFO

Keywords:
Pomegranate peel
HA-PP
Cr (VI) removal
Kinetics
RSM
CCD

ABSTRACT

The present work focuses on preparation of hydroxyapatite from pomegranate peels by precipitation method. The hydroxyapatite derived from pomegranate fruit peels (HA-PP) was characterized by XRD, FT-IR, SEM-EDS and BET techniques. The HA-PP has mesoporous in structure and had an area of 99.021 m^2/g. Further HA-PP was used as adsorbent for the removal of Cr (VI) ion particles from $K_2Cr_2O_7$. The adsorption trials were executed and found the optimized solution using response surface methodology (RSM). The experiments included parameters like pH 2, initial chromium concentration 200 mg/L, adsorbent loading 0.8 g, and contact time 60 min, respectively. Cr (VI) removal was 89.4 % at the optimum combination of these process parameters. A mathematical and statistical optimizing technique response surface methodology (RSM) was applied to verify the interactive effects of various parameters on the adsorption capacity. The analysis of variance (ANOVA) was used to predict the adequacy of the model (F 82.16) shows developed model is valid with R^2 value 0.987, and p-value (>0.1). In this the Langmuir adsorption isotherm and the pseudo-second-order kinetic model are well explained for Cr (VI) adsorption onto HA-PP. This reaction is spontaneous and endothermic, as indicated by the negative change in the standard free energy ($\Delta G^0 = -0.1732$) and ΔH^0 (+4.71) value at the selected temperature. The ΔS^0 (+15.89) further confirms that the randomness increased at the solid-solution interface during adsorption.

1. Introduction

Pomegranate is the ancient eatable fruit having extraordinary nutritional value. The universal cultivation of pomegranate is growing till today; thus, the quantity of fruit peel waste produced is also high [1,2]. In 2017, the global production of this fruit reached almost 3.8 million metric tons (MMT), of which around 1.9 MMT of peels were taken out [3,4]. Punica granatum fruit peels (PFP) containing antioxidant of polyphenolic class which has tannins and flavonoids [5]. Because of this it has been suggested to take part in various pharmacological activities such as anti-aging, anti-inflammatory and anti-atherosclerotic activities [6]. The skin and bark of the pomegranate tree are used as a traditional medication against diarrhea, dysentery and intestinal parasites. Antioxidants contents were as follows: peel > flower > leaf > seed [6]. The PFP shown in Fig. 1.

* Corresponding author.
E-mail address: thomas.theodore@vit.ac.in (T. Theodore).

https://doi.org/10.1016/j.heliyon.2024.e37540
Received 16 July 2024; Received in revised form 30 August 2024; Accepted 4 September 2024
Available online 6 September 2024

Plenty of research work has confirmed the biological properties exist in PFP extracts, signifying their preventive and remedial role in medical pitch [7–9]. Hence, till today in both the developing and developed worlds recommend PFP to treat common health problems [10]. Since huge quantity of waste created, so worthful efforts have been made for the valorisation of PFP [11]; however, a big amount of this waste is still discarded as it is to the environment and it leads to glitches [3]. Hence, in this paper researcher synthesized hydroxyapatite from HA-PP. This hydroxyapatite is a naturally occurring mineral form of calcium apatite with $Ca_{10}(PO_4)_6(OH)_2$ [12]. In the literature plenty of techniques are available for hydroxyapatite (HA) synthesis, those are viz, thermal method or acid treatment [13,14] hydrothermal [15], solid-state reaction [16], chemical precipitation [17], radio frequency thermal plasma [18], and polymer-assisted synthesis method [19]. Among these methods in the present work precipitation method was used for the preparation of hydroxyapatite.

Heavy metal pollution is one of the most important concerns for the environment. Heavy metals such as lead (II) and Ni (II) [20], cadmium (II) [20] arsenic [21] and chromium are continuously discharged into the environment, and these metals are stable and can survive for long time periods in the environment. Among these the Cr (VI) compounds are used in an industrial application such as leather tanning, dyeing, printing, and wood preserving, electroplating, etc. [22–25]. Waste contaminated or polluted water is one of the major issues in the present ecological problems and this waste releases to the environmental [26] and creates various health and ecological problems [27–29]. The most important issues of this pollutant are consisting of bioavailability in the liver, generation of kidney syndromes and death at concentrations higher than 0.1 mg L−1 [30,31].The amount of chromium (VI) ions in different sewage is from 5 to 220 mg L−1, which is much higher than the permitted amount of it in drinking water (0.05 mg L−1) and surface water (0.1 mg L−1) [31,32].

Heavy metals are not biodegradable and can accumulate in living organisms and cause various diseases and disorders in human beings [33,34]. The chromium ions especially Cr(VI) have high toxicity to living organisms. This metal can cause various diseases in human body, such as diarrhea, kidney damage, liver damage, skin cancer [35], respiratory diseases, skin ulcer, nasal congestion, lung cancer [36] and hepatic and stomach injures. In addition, this metal can pass through cell membranes and attack DNA, protein and membrane lipids and damage cell performances and integrity [37].

A number of procedures have been presented for effective treatment for Cr (VI) like adsorption (AP), chemical oxidation, precipitation, lime coagulation, ion exchange, electrodialysis, electrocoagulation [38–42]. Amongst all these methods, AP is one of the most affordable techniques for the removal of Cr (VI) because of its little energy condition, longer effectiveness, ecological and cost requirement is less [43,44]. A wide variety of adsorbents (AB) derived from farming waste [45], bagasse [46], fruit peels [47], vegetable waste [48], straws [49], and some other type of AB like α-Fe2O3 coated hydroxy magnesium silicate (HMS) [50], Artemisia monosperma (AM) powder modified by trimethyloctadecylammonium bromide (TOAB) [51], are found to be highly efficient in Cr (VI) removal. Few AB are alos mentioned for other pollutants viz, CdS@ polysulfone membrane [52] used for wastewater remediating system. , Titanosilicate (TS-SH, TS-SO3H) used for remediation of 1, 4 dioxane from aqueous medium [53], magnetite nanoparticle decorated graphene oxide (MGO) is modified with triethylenetetramine (TETA), which is supported by maleated chitosan (MACS), named MGO@TETA@MACS used for removal of methylene blue dye [54]. Among these, fruit peels have extraordinary consideration because of their profusion, affluence in bioactive compounds, and cost-effective [55].

The novelty of this study is to prepare HA from PFP and evaluate Cr (VI) from synthetic wastewater then optimization study using HA-PP. The XRD proves the formation of HA phase. Several parameters like the effect of, pH, agitation speed (AS), adsorbent loading (AL), contact time (CT), temperature (T), and coexisting ions were considered. From data obtained, isotherms, kinetic models were also evaluated. This study suggests the viability of using PFP as an economical, natural, bio-waste for Cr (VI) sorption, auxiliary the idea of environmental sustainability.

2. Materials and methods

2.1. Hydroxyapatite preparation using pomegranate peel

The HA particles were prepared from PFP. The peels were manually cleaned and washed with water 3–4 times and then cooked in

Fig. 1. Pomegranate waste fruit peel.

water for known period (20 min) and filtered. This filtrate was added to 0.4 M Ca-nitrate tetra hydrate solution and 1:2, 25 % liquor NH_3: H_2O, mixed and incubated for 1d at atmospheric temperature. The obtained liquid was added to 370 mL of 0.156 M $(NH_4)_2HPO_4$ and 30 mL of 1:1, 25 % ammonia: H_2O, mixed and matured for 10–12 days [56]. The precipitate will formed as product i.e HA and this will be washed 4–5 times with deionized H_2O then kept in oven at 80 °C for 24 h [57]. Fig. 2 represents the procedure for the preparation of HA from PFP.

2.2. Batch experiments

The batch experiments were performed using IS 3025 standards [58]. A 1000 mg/L stock solution of Cr (VI) was prepared by dissolving the appropriate amount of potassium dichromate in distilled water. This stock solution was diluted to obtain Cr (VI) solutions of selected concentrations. The pH of the solution was adjusted to required value either by the addition of 0.6 N H_2SO_4. The batch adsorption experiments were carried out using 250-cm^3 Erlenmeyer flasks containing 100 cm^3 of Cr (VI) solution of known concentration to which a known mass of adsorbent is added. The flasks were agitated at 120 rpm on an orbital shaker for a known period of time at 30 °C. The solution was filtered using 0.45-μm syringe filter. The filtered solution was make up to 50 mL with distilled water and adjusted to pH 1.0 using 0.2 N H_2SO_4. A 2 cm^3 of 1,5-Diphenylcarbazide (DPC) was added to the filtered solution which developed a purple colour which is then centrifuged for 20 min at 10,000 rev. min^{-1}. The absorbance of the supernatant is measured at a wavelength of 540 nm using a UV–visible spectrophotometer (Shimadzu UV – 1800) at 540 nm [59]. The batch process for AP study was depicted in Fig. 3. The percentage removal of Cr (VI) was calculated using Eq (1).

$$\% \text{ Removal} = \frac{C0 - Cf}{C0} \times 100 \tag{1}$$

Where, C_0 and C_f (mg/L) are the initial and final concentration of Cr (VI). The amount of Cr (VI) ions adsorbed was determined from Eq. (2).

$$q_e = \frac{(C_i - C_f)}{C_i} \times \frac{V}{m} \tag{2}$$

2.3. Desorption studies

The adsorbents were loaded with toxic heavy metals which generate environmentally hazardous solid spent waste. Therefore, the regeneration of spent materials can make the process cost-effective. A desorption study was conducted using NaOH, HCl and H_2O. Here Cr (VI) contaminated AB treated with selected desorption solutions with a known concentration and kept in orbital shaker for around 30 min with known RPM. After this process it is analysed by standard method IS 3052. Desorption efficiency was estimated from the following standard equation [60]. The process explained as depicted in Fig. 4 [61].

$$\% \text{ Desorption} = \frac{Cd}{Ca} \times 100 \tag{3}$$

3. Results and discussion

3.1. Characterization of the adsorbent

3.1.1. XRD

The HA-PP was subjected to XRD analysis. The schematic diagram displayed in Fig. 5. The peak 112 and main peaks related to (HA-PP) were observed at 2θ values of 25°, 29°, 32°, 40°, and 50°. The Miller indices coordinated well with those of pure HA (JCPDS no. 09–0432), the same are shown in plot.

Miller indices of the major peaks identified for HA-PP, are (002), (112), (202), (222), (213), (310), (411), and (102). These values

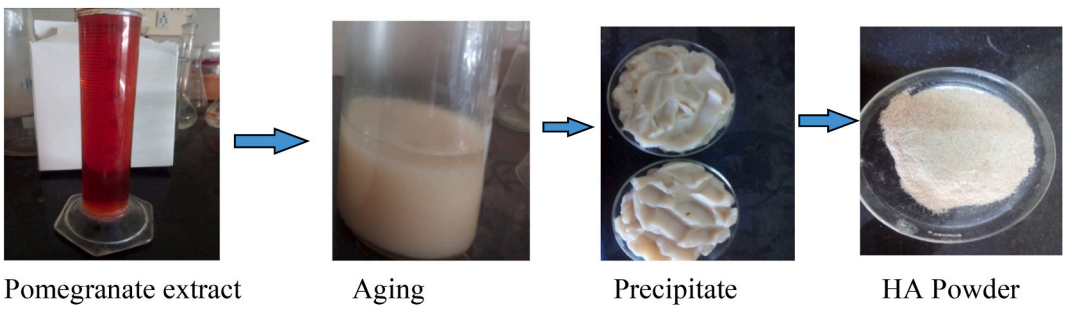

Fig. 2. Procedure for preparation of HA - PP.

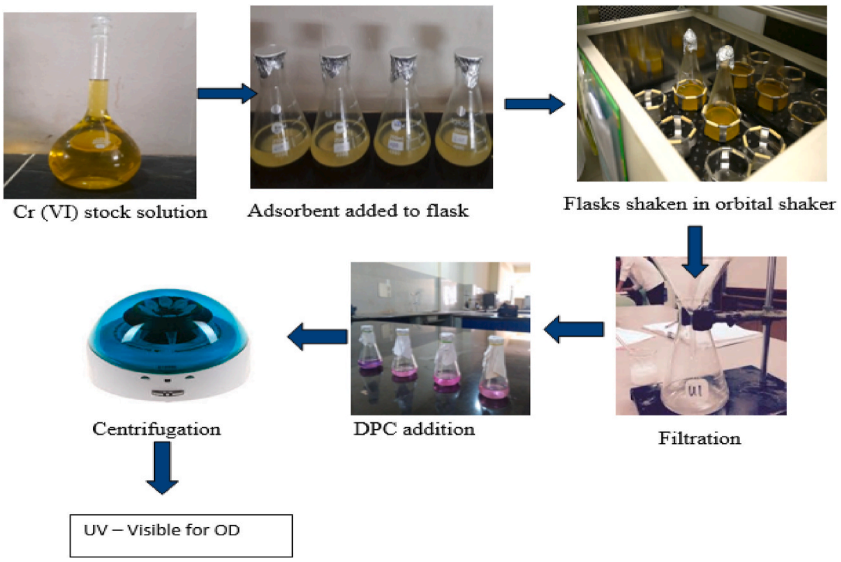

Fig. 3. The process of batch adsorption study of Cr (VI) removal.

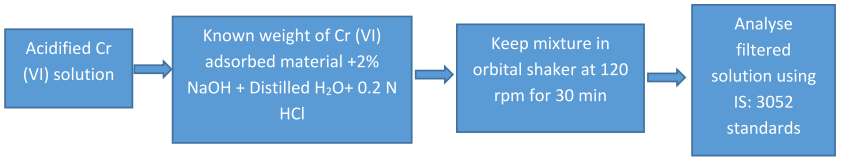

Fig. 4. Process flow sheet of desorption study of HA-PP.

compared very well with the standard XRD data of pure hydroxyapatite (JCPDS No. 09–0432) which confirmed the formation of hydroxyapatite from pomegranate peel. Hence, which confirmed the formation of HA-PP. Equivalent outcomes have been reported by Nayar [56].

3.1.2. FTIR analysis of HA-PP

In Fig. 6 the peaks at 417.8 cm^{-1}, 647.2 cm^{-1}, 723.6 cm^{-1}, and 1147.9 cm^{-1} are due to the distinctive tetrahedral PO_4^{3-} group. These results have been corroborated by Fu et al. and Li et al. [62,63]. The band at 1453.6 cm^{-1} recommended the CO_3^{2-} in the material. The peaks at 1453.6 cm^{-1} and 732.6 cm^{-1} represent the interaction of CO^2 with the HA – PP. Analogous observations were made by Manoj et al. [64,65]. The peaks at 3647.64 cm^{-1} and 3085.77 cm^{-1} are due to the stretching and bending vibrational modes of the OH^- groups of the HA. The change in peaks from 417.8 cm^{-1} to 383.4 cm^{-1}, 647.2 cm^{-1} to 723.6 cm^{-1}, 1147.9 cm^{-1} to 1182.3 cm^{-1}, 1453.6 cm^{-1} to 1335.2 cm^{-1}, and 1633.3 cm^{-1} to 1650.53 cm^{-1} may be due to the Cr (VI) AP on HA-PP.

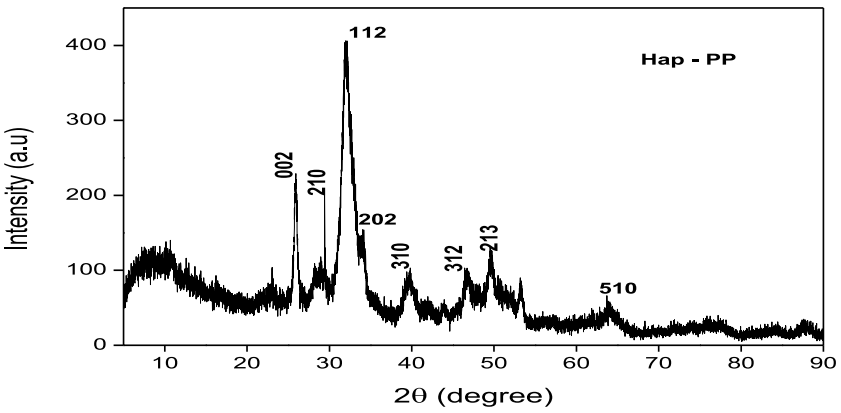

Fig. 5. XRD pattern of HA-PP.

3.1.3. SEM and EDS

Fig. 7 shows presence of Ca and P in the adsorbent. The morphology of HA-PP shows flat luffa like structure [66]. But later Cr (VI) treatment, HA-PP shows crumbling like structure and Cr ions attached to the surface of AB as presented in Fig. 7b and alike results were detected by Dharmawan et al. [67]. Thus, after AP material showed few particles of asymmetrical patches like structure onto the surface HA-PP but it is not in Fig. 7a. The HA-PP was analysed by EDS and is illustrated in Fig. 8.

This study revels presence of Ca (37.46 %) and P (17.01 %), in HA-PP, whereas after contact with Cr (VI), the Ca (34.85 %), P (1.38 %), and Cr (3.15 %) where observed (Fig. 8b). Therefore, the Ca and P after AP the mass lessens because of the contact with the Cr (VI) ion during the AP process. This can be considered as a sign of the interchange of Ca and P with Cr ions onto the HA-PP.

3.1.4. Brunauer-Emmett-Teller (BET) analysis

The BET surface analysis determined the specific surface area, volume, and pore diameter of the HA-PP. The results show the average pore diameter as 24.608 nm which indicates pores are mesoporous having a vast surface area of (99.021 $m^2\ g^{-1}$) [68–70]. However, it is noteworthy that the mesopores play a significant role as the primary pores in the samples [71–73]. A larger specific surface area can provide more active sites [74]. The increase in specific surface area can be attributed to several factors, including the opening of previously inaccessible pores, widening of existing pores, creation of new pores, and integration of existing pores in the structures of the HA-PP similar results reported by Refs. [73,75].

3.2. Batch study

3.2.1. Effect of pH

In this study, trials were planned in the range of 2–8 pH and modifications were done by the addition of 6 M H_2SO_4. The plot for the same is depicted in Fig. 9a. This graph reflects that greater removal of Cr (VI) at (pH 2.0) beneath acidic conditions may be attributed to the charge density (ρ). At pH after 3 and 4, Cr (VI) has a high negative charge due to the presence of oxyanions such as $HCrO_4^-$, $Cr_2O_7^{2-}$ and CrO_4^{2-} in the solution. These ionic forms attach to the surface of material because of H+ ions on the Ha-PP surface. Hence, there is an electrostatic desirability between the (+) charged surfaces of HA-PP and the oxyanions of Cr (VI) [45,46]. As an outcome, the oppositely charged metal ions and the adsorbent's surface declines, and the elimination of Cr (VI) gets reduced radically after pH 2 [76–78].

3.2.2. Effect of agitation speed

Definitely, stirring rate is an influencing parameter in the adsorption mechanism since it is the physical driving force of the process. The maximum removal rate was 90.4 % at 120 rpm. The adsorption capacity of HA-PP constant after RPM increased from 120 to 180 (Fig. 9b). This constant data is due to the saturation of the adsorbent and may be turbulence and did not have enough time to meet the adsorbent surface at higher speeds [79].

3.2.3. Adsorbent loading

The AL was varied from 0.05 to 0.8 g. The results indicated that the removal of Cr (VI) enhances with the improvement in the loading of the adsorbent (AB). Obtained data explains that AL 0.8 g removed 89.8 % of Cr (VI) at 60 min (Fig. 9c). The reason may be due to the fact that a bulky quantity of AL will display additional surface area, which in turn fixes more metal ions, as abundant new binding positions are available for the adsorption, so favouring a high rate of AP [26,78].

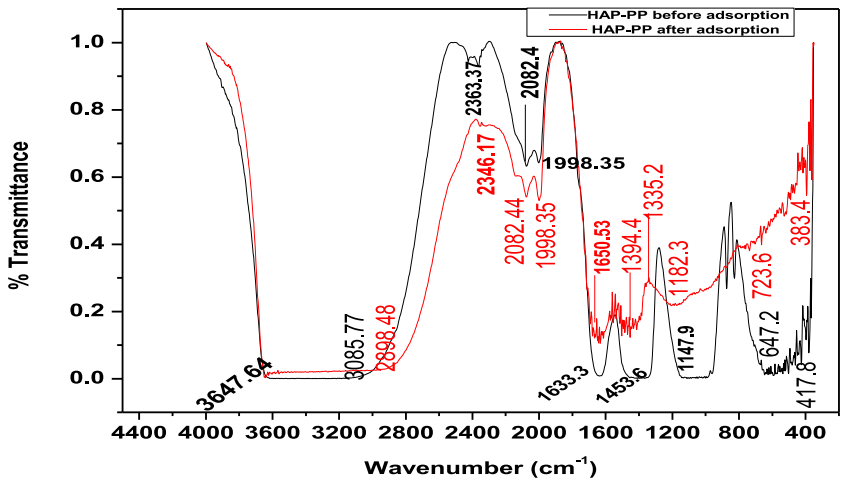

Fig. 6. FTIR plot of HA - PP: (–) before and (–) after Cr (VI) adsorption.

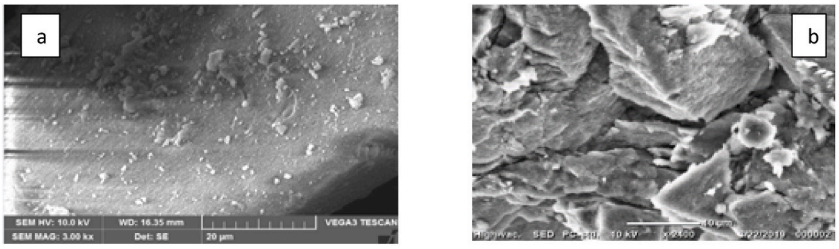

Fig. 7. SEM images of HA - PP.

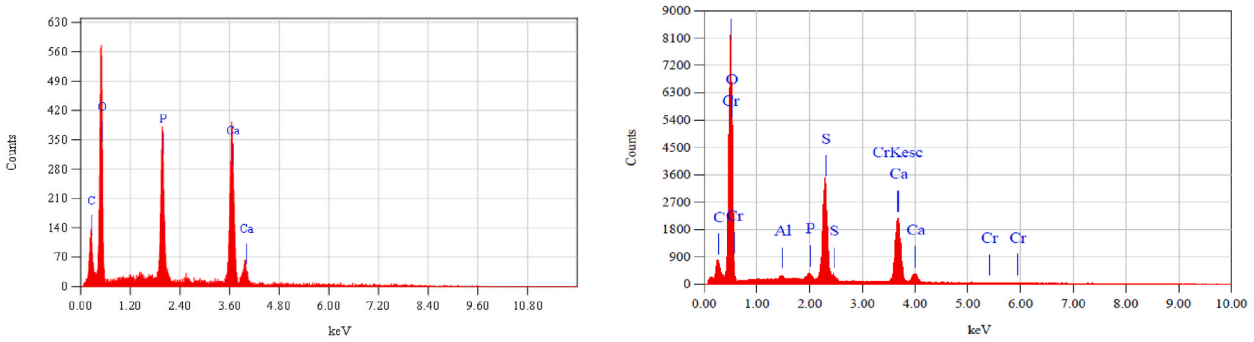

Fig. 8. EDS analysis images of HA - PP (a) before, and (b) after adsorption.

3.2.4. *Effect of temperature*

In this section it was evident that the elimination of Cr (VI) enhances with the rise in temperature (T) from 10 to 50 °C. At 30 °C, the Cr (VI) removal was detected to be 89.91 %, while at 40 °C, 92.8 % removal was noticed (Fig. 9d). At lower T, the kinetic energy of Cr (VI) ruins low; therefore, it becomes hard for Cr (VI) ions to reach the dynamic sites of the AB, whereas, at higher T, the mobility of the metal ions enhances, hence elimination rate was high [80,81].

3.2.5. *Effect of contact time*

The experimental data indicate that Cr (VI) ion AP increased with increasing CT. This is due to prolonged contact between the sorbent surface and the Cr (VI) ion. The Cr (VI) ions enhance as the CT increased from 5 to 60 min. However, no substantial rise in Cr (VI) removal was observed after 30 min (Fig. 9e). The early stage of rate of Cr (VI) AP was found higher due to huge number of energetic obligatory sites present at the exterior surface of the HA-PP and a high concentration gradient [82,83]. After the active sites of the adsorbent gets exhausted, when equilibrium is attained, the rate of uptake is controlled by the rate at which the adsorbate is transported from the exterior to the interior sites of the HA-PP particles.

3.2.6. *Effect of initial concentration*

The IC of the chromium ion plays an important role in determining the removal efficiency of the adsorbent. The adsorption increases initially by increasing the concentration, and reaches to maximum at 200 mg/L (Fig. 9f). The process shows elimination efficiency of Cr (VI) was found to be 89.8 %, at 200 mg/L depicted in (Fig. 9f), while at the lowest concentration, i.e., 50 mg/L, the removal was found to be 43.0 %. The equilibrium was established at 200 mg/L, and there was no further increase in the AP of ions by further increasing Cr (VI) concentration. The ratio of number of moles of Cr (VI) ions to the surface area of AB is large at (200 mg/L), so AP takes place without any interruption. The AB surface area saturates at higher concentration and the ions diffusion from the solution bulk to the adsorbent surface decreases [84,85]. This effect can be ascribed to the enhanced driving force of the mass transport of Cr (VI) molecules towards the active pores within the inner depth of HA-PP at higher initial Cr (VI) concentration [86]. Same results corroborated by Ref. [83].

3.2.7. *Effect of ionic strength*

For the experiment the selected ionic strengths (IS) are (0.1, 0.3, 0.5, 0.7, 10 mol/L). As showed in Fig. 9g, the removal efficiency (57.2 %) was detected at 0.1 M (IS). Enhance in IS, the removal efficacy decline, to 20.9 % represented in (Fig. 9g). The differences in IS of the solution might lead to functional groups available on the AB surface, which probably inhibits with the adsorption process prominent to lesser elimination efficacy [87,88].

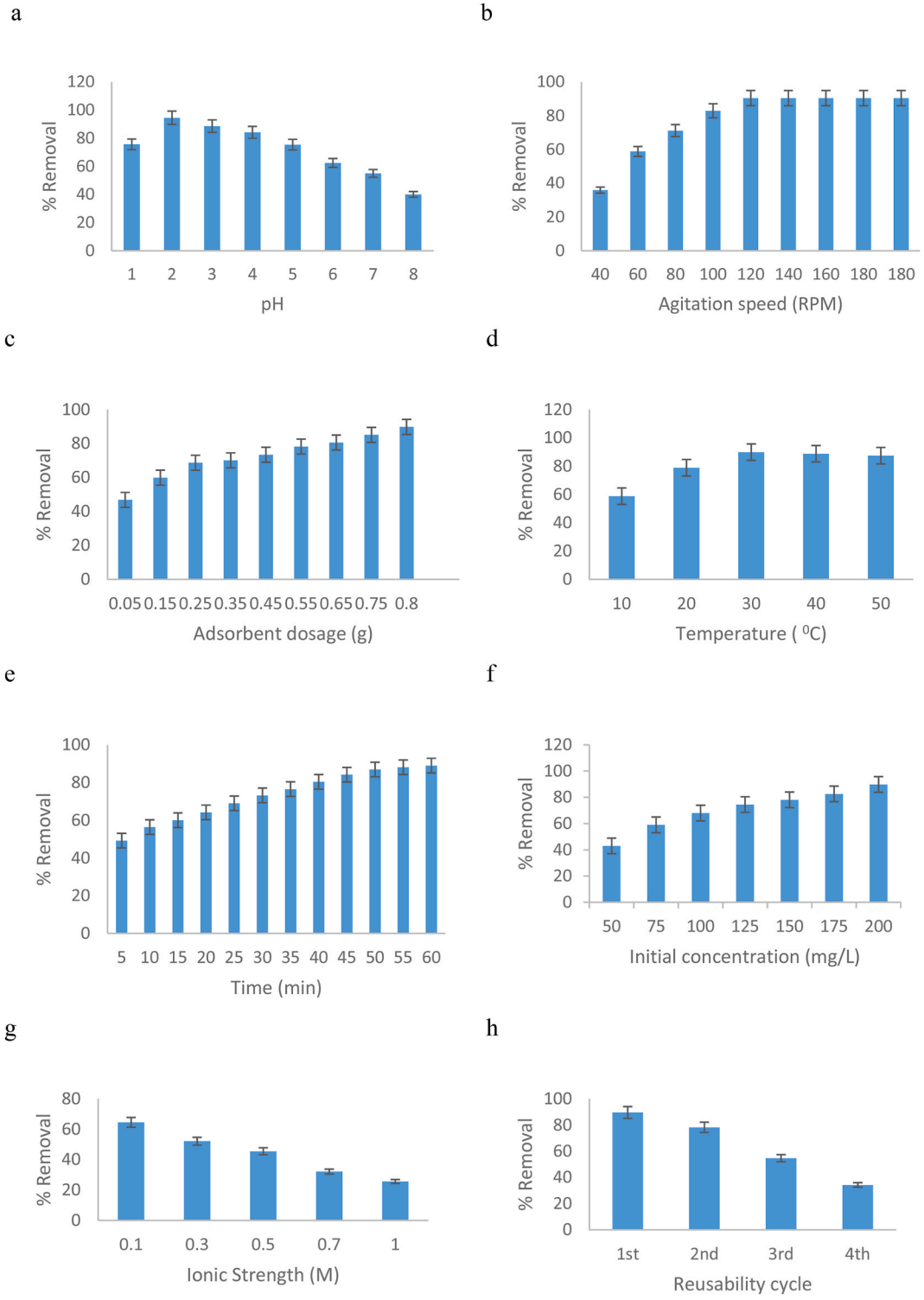

Fig. 9. Effect of a) pH b) agitation speed c) adsorbent dosage d) temperature) contact time f) Initial concentration g) ionic strength and h) Reusability on HA-PP.

3.2.8. Reusability study

The reusability study elaborates, a four consecutive sorption– desorption cycles were performed and the sorption capacity of the material decreased for the certain period. Y. Ren et al., hypothesized that the sorption–desorption process involved complexation,

physisorption and ion exchange reactions [89]. In this study the initial 2 cycles, the AB exhibited more adsorption, i.e., 89.6 % and 84.16 %, but eventually, it slowed down (Fig. 9h), to 75.19 % and 68 % in the III and IV cycle. Here AP followed a declining trend, i.e. (>65 %) for the last two cycles. Finally, material can be reused successfully for Cr (VI) AP up to 5 cycles.

4. Optimization study

RSM was selected for the optimization of the selected parameters for the AP of Cr (VI) by HA-PP. The Design software ® (Stat-Ease Inc., Version 9.0.3.1, Minneapolis, MN) was employed for this purpose. The arrays of the parameters selected were: pH: 2 to 6; AL: 0.05–0.8 g/100 mL, CT: 5–60 min, and IC: 50–200 mg/L. Table, 1 explains the experimental protocol (see Table 1).

Based on percentage AP values analysis will be carried out using analysis of variance ANOVA. The archetypal and lack of fit were tested for importance of the model. The (ANOVA) for the response were shown in Table 2. To check the applicability of the regression model, coefficient of variation (CV%), standard deviation (SD), appropriate precision (AP), and desirability function (DF) were used. It should be noted that the value of DF varies between 0 and 1, and if the value of DF is equal to 1, the answer is favourable, and if the value of DF is equal to 0, the situation is undesirable or has minimal usage.

To confirm the ANOVA results, the normal probability plot of the residual versus the histogram of the residual was used. The obtained data were in line with one line, which shows that the data is normal and the results of ANOVA are valid [90]. The Cox-Box diagram is a tool that is analysed in the regression analysis of RSM-CCD data and how well the experimental data match the equation. This technique helps to stabilize variance and can improve the accuracy of any subsequent statistical tests or models.

This plot is used to determine the most appropriate transfer function to apply to the specified responses. Based on the Cox-Box diagram, the best lambda value for HA-PP was determined to be 1 (Fig. 10). The results showed that the experimental data for the Cr (VI) treatment process do not need to be transferred to promote the model and have sufficient accuracy. Similar results shown by Refs. [90,91].

The F value of 82.16 suggests the model is significant. There is only a 0.01 % chance that an F-value this high could occur due to noise. The p (prob $> F < 0.05$) indicates model terms are significant. In this case, A, B, C, D, AB, and A^2 are significant and p-value (>0.1) shows model terms are not significant. The predicted R^2 value of 0.9311 is in reasonable agreement with the adjusted (R^2 - 0.9751): i.e., the difference is (< than 0.044). Adequate precision measures the range of the predicted value at the design points to the average prediction error. A signal to noise ratio (>4.0) hence model is adequate [92]. Fig. 10 shows the 3-D response surface plots of Cr (VI) adsorption on HA-PP.

The superlative conditions for the AP of Cr (VI) onto HA-PP adsorbent determined using the CCD are pH: 2, AD: 0.8 g/100 mL, IC: 200 mg/L, and CT: 60 min for a maximum Cr (VI) removal of 89.4 %.

Table 1
Optimization study plan generated by Design-Expert ® software for HA-PP.

A: pH	B: AD (g/100 mL)	C: CT	D: IC	% AP
4	0.05	32.5	125	73.33
4	0.425	32.5	125	75.6
6	0.8	5	50	55.27
4	0.425	32.5	125	76.2
2	0.8	60	200	89.4
4	0.425	32.5	200	84.21
2	0.05	5	50	57.3
4	0.425	5	125	70.1
2	0.8	5	50	64.3
4	0.425	32.5	125	77.9
6	0.8	60	200	82.4
6	0.8	5	200	79.9
6	0.05	60	200	80.4
4	0.425	32.5	125	76.92
4	0.425	60	125	78.9
2	0.8	60	50	67.2
2	0.05	60	50	64.4
2	0.05	60	200	82.92
4	0.425	32.5	125	75.9
6	0.05	5	200	73.6
2	0.05	5	200	78
4	0.8	32.5	125	77.05
6	0.05	60	50	62.4
6	0.05	5	50	55.89
4	0.425	32.5	50	67.8
6	0.425	32.5	125	71.1
6	0.8	60	50	61.6
4	0.425	32.5	125	74.92
2	0.425	32.5	125	77.1
2	0.8	5	200	83.24

Table 2
ANOVA response for HA-PP.

Source	Sum of squares	Degree of freedom (df)	Mean square	F-value	p-value (prob > F)	Significance (S)
Model	2238.73	14	159.91	82.16	<0.0001	S
A – pH	94.76	1	94.76	48.69	<0.0001	
B - AD	57.32		57.32	29.45	<0.0001	
C - CT	150.34		150.34	77.24	<0.0001	
D - IC	1758.44		1758.44	903.45	<0.0001	
AB	13.40		13.40	6.88	0.0192	
AC	0.070		0.070	0.036	0.8519	
AD	0.038		0.038	0.020	0.8907	
BC	3.46		3.46	1.78	0.2024	
BD	8.47		8.47	4.35	0.0545	
CD	0.38		0.38	0.19	0.6656	
A^2	11.67		11.67	5.99	0.0271	
B^2	2.76		2.76	1.42	0.2522	
C^2	7.68		7.68	3.95	0.0655	
D^2	0.12		0.12	0.063	0.8056	
Residual	29.20	15	1.95			
Lack of Fit	23.71	10	2.37	2.16	0.2045	Not significant
Pure Error	5.49	5	1.10			
Corrected Total	2267.93	29	R-Squared		0.9871	
Std. Deviation	1.40		Adj R^2		0.9751	
Mean	73.17		Pred R^2		0.9311	
C.V %	1.91		Adeq Precision		34.167	

5. Adsorption isotherm

The results elaborate R^2 (0.973) of the Langmuir AP isotherm for HA-PP were found to be grater then the other isotherms (Fig. 11).

The K_a and q_m were obtained from the slope and the intercept of a linear plot of 1/qe versus $1/C_e$ displayed in (Table 3). The good fit of the Langmuir isotherm indicates the development of a Cr layer on the outer face of the AB [93]. In this case, the R_L lies between 0 and 1 revels that the process is favourable [94]. Langmuir isotherm model postulates the equivalence of energy for the adsorbent sites all over the adsorbent surface. This surface homogeneity enables adsorbate to be adsorbed within monolayer behavior [95,96]. Therefore, more sorption are prohibited at these sites. For more justification of Cr(VI) adsorption, sorption results were further fitted using Freundlich equation. At equilibrium, Freundlich isotherm assumes the occurring of adsorption on adsorbent's surface of non-uniform heterogeneity. From the slope and intercept evaluated from the linear plotting of log qe against log Ce, the parameters of Freundlich equation are estimated and illustrated in Table 3. The values of ''n = 0.02″ that reflects some surface heterogeneity and adsorption favorability with condition $0 < n < 1$ [97,98]. Additionally, the R^2 of average value (0.9545) for the linearity of Freundlich equation shows a good fitting. A value near to 0 indicates a heterogeneous surface. A value < 1 shows chemisorption [97].

For the D-R isotherm, the slope (S) of a plot of ln q_e versus ε^2 gives β (mol^2/kJ^2) and the intercept (I) yields the AP capacity, q_m (mol/g). The D-R constants are tabulated in Table 3. The Temkin constants A_T and B_T were found from the slope and intercept of a plot of qe against ln C_e. More adsorption at the expense of less energy was evident from the q_m (0.66) mg. $g^{-1}$and K_a (0.0085) L.mg^{-1} [99]. In addition, the value of the B_T parameter was quantified to be < 1 kJ/mol, which emphasizes that physical adsorption has occurred and the interaction between adsorbers and Cr (VI) is controlled by electrostatic force [100,101].

6. Adsorption kinetics

In order to design and model the sorption process, the kinetic parameters were determined. Also, they were used for selecting the most advantageous working conditions for a full-scale batch process. It is well known that the sorption mechanism may involve three processes or their combination: surface adsorption, chemical interaction and diffusion. The slowest of these processes determines the rate limiting step. In order to identify the kinetic order and the rate limiting step, the experimental data was processed using 4 of the most widely used adsorption kinetic models. The kinetic parameters related to each model, calculated from the intercepts and slopes of the corresponding linear plots. The fitting of each model to the experimental data was estimated using the regression correlation coefficient, R^2 value.

A straight line of $1/q_t$ versus 1/t suggests the applicability of the first-order kinetic model (Fig. 12a). q_1 and k_1 were determined from the intercept and slope of the plot and the values are presented in Table 4.

The plot of t/q_e versus time (t) (Fig. 12b) yielded a straight line which suggests the applicability of the pseudo-2nd-order model (PSOM). The constants q_2 and k_2 were determined from the intercept and slope of the plot. From the data, the calculated and experimental q_e values are seen to be in good agreement with each other. The maximum Cr (VI) adsorption capacity was found to be 8.98 mg g^{-1}. The PSOM gave the highest R^2 value for HA-PP. Thus, it concludes that the AP process obeys the PSOM [102]. The assumption of PSOM is the rate-limiting phase may be chemical AP connecting valence forces through distribution or interchange of electrons among the AB and the adsorbate [99].

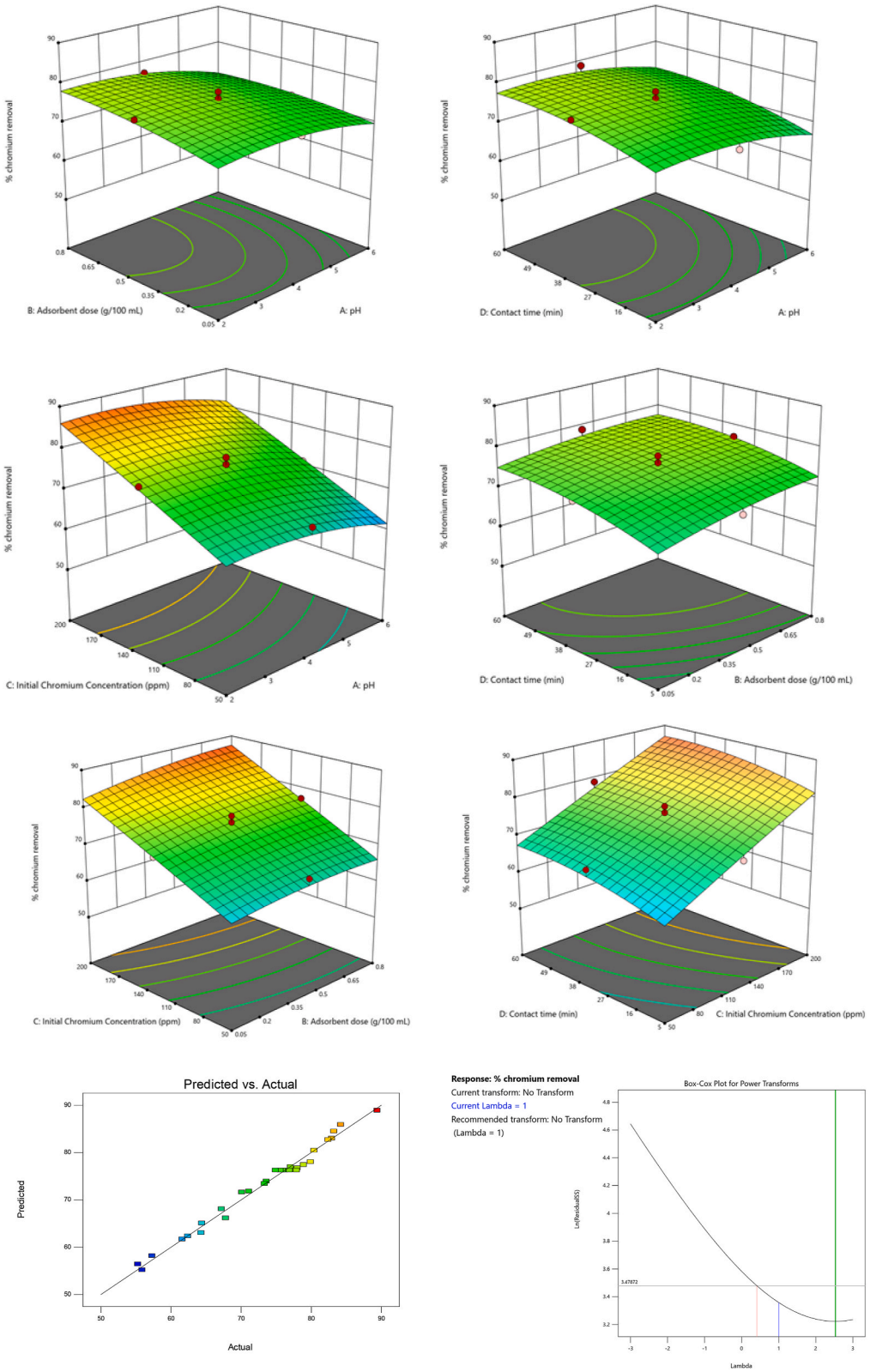

Fig. 10. 3-D response surface plots and Box-Cox plot of HA-PP adsorbent.

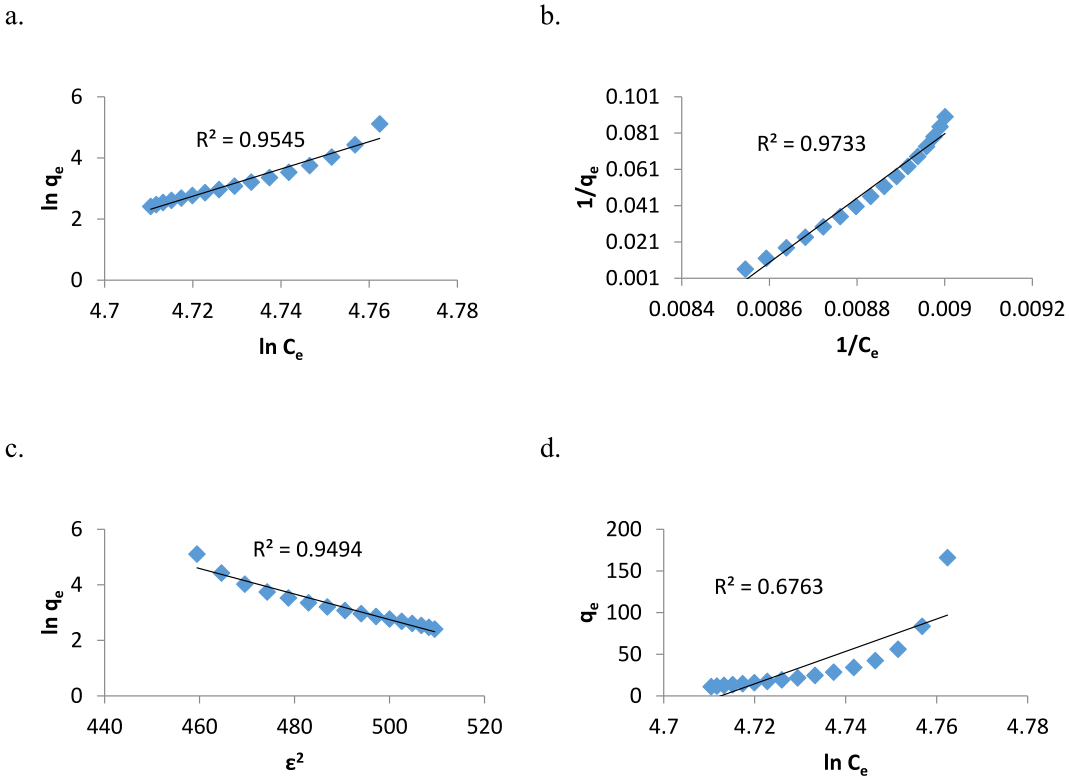

Fig. 11. (a) Freundlich, (b) Langmuir, (c) D-R, and (d) Temkin isotherms of HA - PP.

Table 3
Summary of the isotherm constants.

Freundlich:		Temkin:	
S: 1/n	44.59	S: B (J.mol^{-1})	1945.17
I: ln K_f	207.74	I: B ln A_T	−9166.71
n	0.02	B_T	1.29
K_f	6.01 × 10^{-91}	A_T	0.0089
R^2	0.954	R^2	0.924
Langmuir:		**D-R:**	
S: 1/q_mK_a	177.29	S: K_{ad}	−0.045
I: 1/q_m	1.51	I: lnq_s	25.74
q_m (mg.g^{-1})	0.66	q_s (mg.g^{-1})	6.9 × 10^{69}
K_a (L.(mg)$^{-1}$)	0.0085	E (KJ/mol^2)	0.150
R_L	0.65	R^2	0.949
R^2	0.973		

In the present study, for the intraparticle diffusion model, the adsorbents showed R^2 values for HA-PP ($R^2 = 0.930$) and the lines do not pass through the origin which is an indication that the model appropriate to explain HA-PP adsorption kinetics.

Elovich model, a plot of q_e v/s ln (t) Fig 12 (d) must give a straight line of slope, 1/β and intercept, 1/β ln (αβ) [103] presented in Table 4. The high values of $R^2 > 0.9$ reveal good fitting for the Elovich equation with great possibility for mass transfer when describing the chemisorption on heterogeneous adsorbent [104]. According to the obtained results of adsorption kinetics, the Cr(VI) adsorption on HA-PP surface best rendered to pseudo second-order kinetics in addition to the Elovich kinetic model within the frame of chemisorption mechanism. Similar results reported by Ref. [51]. The constant were presented in Table 4.

7. Temperature study

To explore the feasibility of Cr (VI) uptake by the HA-PP, the thermodynamic variables ΔG^0 (Eq. (4), ΔH^0 (), and ΔS^0 (Eq. (5)) were determined.

$$\Delta G = - RTlnK \quad (4)$$

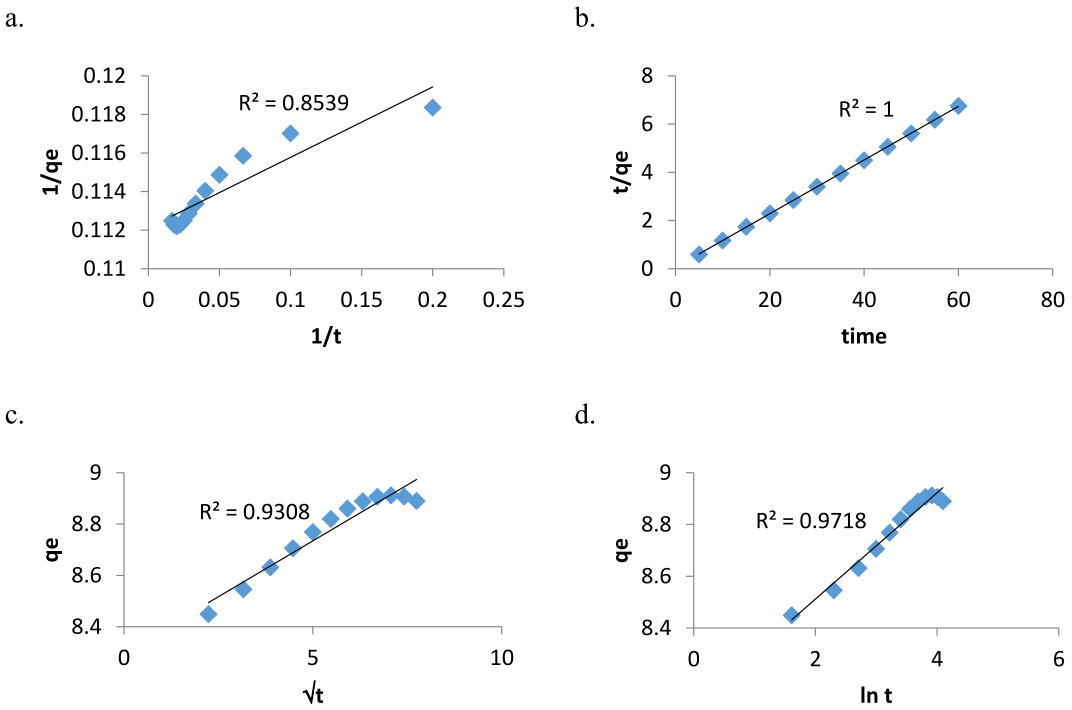

Fig. 12. (a) First-order, (b) pseudo-2nd-order, (c) intraparticle diffusion, and (d) Elovich models for HA - PP.

Table 4
Adsorption kinetic parameters for HA-PP.

First-order		Pseudo-second-order	
k_1 ($l.min^{-1}$)	0.036	k_2 (g/mg.min)	0.21
q_1 ($mg.g^{-1}$)	0.11	q_2 ($mg.g^{-1}$)	8.98
R^2	0.853	R^2	1.0
Intraparticle diffusion		**Elovich**	
k_{id} ($mg/g.min^{1/2}$)	0.087	α (mg/g.min)	0.25
C	8.29	β (g/mg)	4.86
R^2	0.930	R^2	0.971

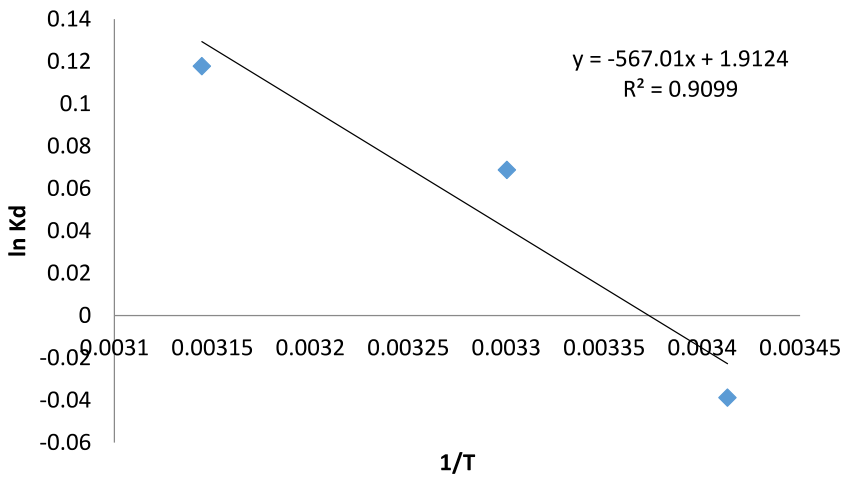

Fig. 13. Plot of ln K_d vs. 1/T for the estimation of the thermodynamic parameters for the adsorption of Cr (VI) on the HA-PP.

$$\ln K_c = \frac{-\Delta H}{RT} + \frac{\Delta S}{R} \quad (5)$$

Where, Kc is the thermodynamic constant, which is equal to qe/Ce. The ΔH^0 and ΔS^0 of the removal process were estimated from the intercept and slope of the plot of ln Kc against 1/T (Fig. 13). As the adsorption temperature increased, the values of *kd* increased as well, indicating that the Cr (VI) adsorption capacity increased with the rise of temperature and this suggested that the adsorption process was an endothermic in nature. The negative ΔG° values advocated that the adsorption process was spontaneous and more favourable at low temperature [105,106]. The positive value of ΔH° (4.71 kJ/mol) confirmed the endothermic nature of the adsorption process and the positive ΔS° (15.89 J/mol K) value revealed the increase in the randomness at solid–solution interface.

There is unequal release of energy during the adsorption process and the magnitude of ΔH° value offers information about the forces that governed the adsorption process. In this work, the ΔH° value was found to be 4.71 kJ/mol, this confirming that it is physical forces were involved in the adsorption of Cr (VI) onto HA-PP. Similar results corroborated by Refs. [86,107,108].

8. Mechanism of adsorption

The heavy metal AP from wastewaters by AB involves a variety of mechanisms such as electrostatic interactions between metal and the functional surface of the material, cation exchange between metals and alkaline metals on the material surface, metal precipitation, and metal reduction followed by sorption, and metal complexation of the HA-PP. This process of separation, implies the transfer of adsorbate (i.e., pollutant) from the fluid (i.e., synthetic solution) to the surface of a solid matrix (i.e., adsorbent) that should have a tailored surface chemistry and porosity to reach an effective separation. It also offers the possibility to recover the adsorbate (s) loaded on the AB surface via desorption thus facilitating the AB recycling. The effectiveness of AP of Cr (VI) ions is affected by several operating variables like CT, AL, temperature, IC, and pH. Also, textural parameters and surface functionalities of the material used as an adsorbent are paramount to achieve a successful removal of Cr (VI). The exploration of the adsorption mechanisms of Cr^{6+} through adsorption thermodynamics and adsorption kinetics has become the primary focus of research. The mechanisms of adsorption by the adsorbents were all consistent with the PSO kinetic model, indicating the adsorption of Cr^{6+} by these materials occurs by chemisorption. Some isotherm types conform to the Langmuir equation, and some conform to the Freundlich equation, depending on the heterogeneity of the adsorbent surface. Therefore, it is important to characterize, assess, and model the performance of low-cost materials as adsorbents for the removal of Cr (VI) ions at different operating conditions with the aim of identifying the best alternatives for real-life and industrial applications [109].

9. Conclusion

The adsorptions of Cr (VI) onto the HA-PP were inveterate by the characterization of the material by XRD, FT-IR, SEM-EDS and BET. The optimized parameters for HA-PP: pH 2, AL 0.8g, IC 200 mg. L^{-1}, CT 60 min, AS, and IS studied and removal found to be 89.4 %. In CCD of RSM the models F-value specify that the models are significant. Values of $P > F < 0.0001$ terms revels model are significant. The predicted R^2 is in reasonable agreement with the adjusted R^2. The 3D plots elucidate the collective effects of all the parameters on the AP. ANOVA study showed that the models were significant to fit the data. The statistics fitted well with the Langmuir isotherm and pseudo-2nd-order kinetic models. The reusability experiments indicated that the HA-PP could be reused effectively up to 4 cycles. Thus, it can be concluded that HA-PP are good and eco-friendly adsorbent.

CRediT authorship contribution statement

Suman Pawar: Writing – original draft, Validation, Software, Methodology, Data curation. **Thomas Theodore:** Writing – review & editing, Validation, Methodology, Conceptualization.

Declaration of competing interest

We wish to confirm that there are no known conflicts of interest associated with this publication and there has been no significant financial support for this work that could have influenced its outcome.

References

[1] S. Ben-Ali, Application of raw and modifed pomegranate peel for wastewater treatment: a literature overview and analysis, Int. J. Chem. Eng. (2021) 8840907, https://doi.org/10.1155/2021/8840907.
[2] N.B. Hasnaoui, A. Wathelet, Jiménez-Araujo, Valorization of pomegranate peel from 12 cultivars: dietary fbre composition, antioxidant capacity and functional properties, Food Chem. 160 (2014) 196–203, https://doi.org/10.1016/j.foodchem.2014.03.089.
[3] E.I. Barnossi, A. Moussaid, Iraqi Housseini, F.A. Tangerine, Banana and pomegranate peels valorisation for sustainable environment: a review, Biotechnol Rep 29 (2021) e00574, https://doi.org/10.1016/j.btre.2020.e00574.
[4] H. Saad, F. Charrier-El, F. Bouhtoury, A.P. Pizzi, K. Rode, B. Charrier, N. Ayed, Characterization of pomegranate peels tannin extractives, Ind. Crops Prod. 40 (2012) 239–246, https://doi.org/10.1016/j.indcrop.2012.02.038.
[5] T.A. El-Desouky, M.R. Sherif, M.S. Sherif, N.M. Khayria, Protective effect of aqueous extract pomegranate peel against sterigmatocystin toxicity in rat, J. Drug Deliv. Therapeut. 5 (2015) 9–18, https://doi.org/10.22270/jddt.v5i5.1136.

[6] M.I. Gil, F.A. Tomas-Barberan, B. Hess-Pierce, D.M. Holcroft, A.A. Kader, Antioxidant activity of pomegranate juice and its relationship with phenolic composition and processing, J. Agric. Food Chem. 48 (2000) 4581–4589.
[7] N.S. Al-zoreky, K. Nakahara, Antibacterial activity of extracts from some edible plants commonly consumed in Asia, Int. J. Food Microbiol. 80 (2003) 223–230.
[8] N. Arun, D.P. Singh, Punica granatum: a review on pharmacological and therapeutic properties, Int. J. Pharmaceut. Sci. Res. 3 (5) (2012) 1240–1245.
[9] P.S. Negi, G.K. Jayaprakasha, Antioxidant and antibacterial activities of Punica granatum peel extracts, Food Microbiology and Safety 68 (2003) 1473–1477.
[10] T. Ismail, P. Sestili, S. Akhtar, Pomegranate peel and fruit extracts: a review of potential anti-inflammatory and anti-infective effects, J. Ethnopharmacol. 143 (2) (2012) 397–405.
[11] R.K. Pal, J. Sharma, D. Babu, N. Singh, N. Gaikwad, Pomegranate Revolution in India a Success Story of ICAR, ICAR-NRC on Pomegranate, Solapur, 2017, p. 14.
[12] A. Singh, A. Tiwari, J. Bajpai, A.K. Bajpai, Biomaterials: from Action to Application, Handbook of Antimicrobial Coatings, Elsevier, Amsterdam, The Netherlands, 2017, p. 27.
[13] R. Chakraborty, S. Bepari, A. Banerjee, Application of calcined waste fish (Labeo rohita) scale as low-cost heterogeneous catalyst for biodiesel synthesis, Bioresour. Technol. 102 (3) (2011) 3610–3618, https://doi.org/10.1016/j.biortech.2010.10.123.
[14] S. Kongsri, K. Janpradit, K. Buapa, S. Techawongstien, S. Chanthai, Nanocrystalline hydroxyapatite from fish scale waste: preparation, characterization and application for selenium adsorption in aqueous solution, Chem. Eng. J. 215 (2013) 522–532, https://doi.org/10.1016/j.cej.2012.11.054.
[15] Y. Azis, N. Jamarun, S. Arief, H. Nur, Facile synthesis of hydroxyapatite particles from cockle shells (Anadaragranosa) by hydrothermal method, Orient. J. Chem. 31 (2) (2015) 1–7, https://doi.org/10.13005/ojc/310261.
[16] S.H. Rhee, Synthesis of hydroxyapatite via mechanochemical treatment, Biomaterials 23 (4) (2002) 1147–1152, https://doi.org/10.1016/S0142-9612(01)00229-0.
[17] Y.X. Pang, X. Bao, Influence of temperature, ripening time and calcination on the morphology and crystallinity of hydroxyapatite nanoparticles, J. Eur. Ceram. Soc. 23 (10) (2003) 1697–1704, https://doi.org/10.1016/S0955-2219(02)00413-2.
[18] J.L. Xu, K.A. Khor, Z.L. Dong, Y.W. Gu, R. Kumar, P. Cheang, Preparation and characterization of nano-sized hydroxyapatite powders produced in a radio frequency (rf) thermal plasma, Mater. Sci. Eng., A 374 (1–2) (2004) 101–108, https://doi.org/10.1016/j.msea.2003.12.040.
[19] Y.H. Tseng, C.S. Kuo, Y.Y. Li, C.P. Huang, Polymer-assisted synthesis of hydroxyapatite nanoparticle, Mater. Sci. Eng. 29 (3) (2009) 819–822, https://doi.org/10.1016/j.msec.2008.07.028. C.
[20] R. Foroutan, H. Esmaeili, A.M. Sanati, M. Ahmadi, B. Ramavandi, Adsorptive removal of Pb (II), Ni (II), and Cd (II) from aqueous media and leather wastewater using Padinasanctae-crucis biomass, Desalin Water Treat 135 (2018) 236–246, https://doi.org/10.5004/dwt.2018.23179.
[21] H. Xiong, S. Xu, S. Zhu, Adsorption removal of arsenic from aqueous solutions and groundwater by isomeric FeOOH, Water Sci. Technol. 86 (7) (2022) 1653–1667, https://doi.org/10.2166/wst.2022.303.
[22] R. Singh, V. Misra, R.P. Singh, Removal of hexavalent chromium from contaminated ground water using zero-valent iron nanoparticles, Environ. Monit. Assess. 184 (6) (2012) 3643–3651, https://doi.org/10.1007/s10661-011-2213-5.
[23] M.H. Dehghani, M.M. Taher, A.K. Bajpai, B. Heibati, I. Tyagi, M. Asif, S. Agarwal, V.K. Gupta, Removal of noxious Cr (VI) ions using single-walled carbon nanotubes and multi-walled carbon nanotubes, Chem Eng J 279 (2015) 344–352, https://doi.org/10.1016/j.cej.2015.04.151.
[24] F. Mutongo, O. Kuipa, P.K. Kuipa, Removal of Cr(VI) from aqueous solutions using powder of potato peelings as a low cost sorbent, Bioinorg Chem Appl 2014 (2014) 973153, https://doi.org/10.1155/2014/973153.
[25] S. Rafaee, M.R. Samani, D. Toghraie, Removal of hexavalent chromium from aqueous media using pomegranate peels modifed by polymeric coatings: effects of various composite synthesis parameters, Synth. Met. 265 (2020) 116416, https://doi.org/10.1016/j.synthmet.2020.116416.
[26] T. Mohammed, R. Ibrahim, A. Naji, Experimental investigation and thermodynamic study of heavy metal removal from industrial wastewater using pomegranate peel, MATEC Web Conf 162 (2018) 05007, https://doi.org/10.1051/matecconf/201816205007.
[27] A.M. Bobaker, I. Alakili, S.B. Sarmani, N. Al-Ansari, Z.M. Yaseen, Determination and assessment of the toxic heavy metal elements abstracted from the traditional plant cosmetics and medical remedies: case study of Libya, Int. J. Environ. Res. Publ. Health 16 (2019) 11 1957–1966, https://doi.org/10.3390/ijerph16111957.
[28] A. Elzwayie, A. El-shafie, Z.M. Yaseen, H.A. Afan, M.F. Allawi, RBFNN-based model for heavy metal prediction for different climatic and pollution conditions, Neural Comput. Appl. 23 4 (2016) 423–433, https://doi.org/10.1007/s00521-015-2174-7.
[29] S.K. Bhagat, T.M. Tung, Z.M. Yaseen, Development of artificial intelligence for modeling wastewater heavy metal removal: state of the art, application assessment and possible future research, J. Clean. Prod. 13 (7) (2019) 469–473, https://doi.org/10.1016/j.jclepro.2019.119473.
[30] R.M. Schneider, C.F. Cavalin, M.A.S.D. Barros, C.R.G. Tavares, Adsorption of chromium ions in activated carbon, Chem. Eng. J. 132 (1–3) (2007) 355–362, https://doi.org/10.1016/j.cej.2007.01.031.
[31] Y. Abshirini, H. Esmaeili, R. Foroutan, Enhancement removal of Cr (VI) ion using magnetically modified MgO nanoparticles, Mater. Res. Express 6 (12) (2019) 125513.
[32] Y. Wang, D. Liu, J. Lu, J. Huang, Enhanced adsorption of hexavalent chromium from aqueous solutions on facilely synthesized mesoporous iron–zirconium bimetal oxide, Colloids Surf. A Physicochem. Eng. Asp. 481 (2015) 133–142, https://doi.org/10.1016/j.colsurfa.2015.01.060.
[33] W. Peng, H. Li, Y. Liu, S. Song, A review on heavy metal ions adsorption from water by graphene oxide and its composites, J. Mol. Liq. 230 (2017) 496–504, https://doi.org/10.1016/j.molliq.2017.01.064.
[34] R. Foroutan, R. Mohammadi, B. Ramavandi, Treatment of chromium-laden aqueous solution using $CaCl_2$-modified Sargassum oligocystum biomass: characteristics, equilibrium, kinetic, and thermodynamic studies, Kor. J. Chem. Eng. 35 (2018) 234–245, https://doi.org/10.1007/s11814-017-0239-2.
[35] N. Ballav, H.J. Choi, S.B. Mishra, A. Maity, Polypyrrole-coated halloysite nanotube clay nanocomposite: synthesis, characterization and Cr (VI) adsorption behaviour, Appl. Clay Sci. 102 (2014) 60–70, https://doi.org/10.1016/j.clay.2014.10.008.
[36] S. Kuppusamy, P. Thavamani, M. Megharaj, K. Venkateswarlu, Y.B. Lee, R. Naidu, Potential of Melaleuca diosmifolia leaf as a low-cost adsorbent for hexavalent chromium removal from contaminated water bodies, Process Saf. Environ. Protect. 100 (2016) 173–182, https://doi.org/10.1016/j.psep.2016.01.009.
[37] H.C. Vu, A.D. Dwivedi, T.T. Le, S.H. Seo, E.J. Kim, Y.S. Chang, Magnetite graphene oxide encapsulated in alginate beads for enhanced adsorption of Cr (VI) and as (V) from aqueous solutions: role of crosslinking metal cations in pH control, Chem. Eng. J. 307 (2017) 220–229, https://doi.org/10.1016/j.cej.2016.08.058.
[38] V.K. Gupta, R. Prasad, P. Kumar, R. Mangla, New nickel(II) selective potentiometric sensor based on 5,7,12,14-tetramethyldibenzotetraazaannulene in a poly (vinyl chloride) matrix, Anal. Chim. Acta 420 (2000) 19–27, https://doi.org/10.1016/S0003-2670(00)01013-8.
[39] V.K. Gupta, A.K. Jain, G. Maheshwari, Aluminum (III) selective potentiometric sensor based on morin in poly(vinyl chloride) matrix, Talanta 72 (2007) 1469–1473, https://doi.org/10.1016/j.talanta.2007.01.064.
[40] C.A. Kozlowski, W. Walkowiak, Removal of chromium (VI) from aqueous solutions by polymer inclusion membranes, Water Res. 36 (2002) 4870–4876, https://doi.org/10.1016/S0043-1354(02)00216-6.
[41] D. Park, Y.S. Yun, J.Y. Kim, J. Park, How to study Cr(VI) biosorption: use of fermentation waste for detoxifying Cr(VI) in aqueous solution, Chem Eng J 136 (2008) 173–179, https://doi.org/10.1016/j.cej.2007.03.039.
[42] C. Rizzo, J.L. Andrews, J.W. Steed, F. D'Anna, Carbohydrate supra molecular gels: adsorbents for chromium(VI) removal from wastewater, J. Colloid Interface Sci. 548 (2019) 184–196, https://doi.org/10.1016/j.jcis.2019.04.034.
[43] A. Ajmani, T. Shahnaz, S. Narayanan, S. Narayanasamy, Equilibrium, kinetics and thermodynamics of hexavalent chromium biosorption on pristine and zinc chloride activated Senna siamea seed pods, Chem. Ecol. 35 (2019) 379–396, https://doi.org/10.1080/02757540.2019.1584614.
[44] G. Bharath, K. Rambabu, F. Banat, A. Hai, A.F. Arangadi, N. Ponpandian, Enhanced electrochemical performances of peanut shell derived activated carbon and its Fe3O4 nanocomposites for capacitive deionization of Cr (VI) ions, Sci. Total Environ. 691 (2019) 713–726, https://doi.org/10.1016/j.scitotenv.2019.07.069.

[45] I. Zinicovscaia, D. Grozdov, N. Yushin, D. Abdusamadzoda, S. Gundorina, E. Rodlovskaya, O. Kristavchuk, Metal removal from chromium containing synthetic effluents by Saccharomyces cerevisiae, Desalination Water Treat. 178 (2020) 254–270, https://doi.org/10.5004/dwt.2020.24987.

[46] A. Ali, K. Saeed, F. Mabood, Removal of chromium (VI) from aqueous medium using chemically modifed banana peels as efcient, low-cost adsorbent, Alex. Eng. J. 55 (2016) 2933–2942, https://doi.org/10.1016/j.aej.2016.05.011.

[47] O. Ekpete, F. Kpee, J. Amadi, R. Rotimi, Adsorption of chromium (VI) and zinc(II) ions on the skin of orange peels (Citrus sinensis), J. Nepal Chem. Soc. (2010), https://doi.org/10.3126/jncs.v26i0.3628.

[48] F. Mutongo, O. Kuipa, P.K. Kuipa, Removal of Cr(VI) from aqueous solutions using powder of potato peelings as a low cost sorbent, Bioinorg Chem Appl 2014 (2014) 973153, https://doi.org/10.1155/2014/973153.

[49] M. Shadreck, F. Chigondo, M. Shumba, C. Benias, E. Nyamunda, E. Dube, Removal of chromium (VI) from aqueous solution using chemically modifed orange (Citrus cinensis) peel, IOSR J. Appl. Chem. 6 (2013) 66–75.

[50] M.S. Alshammari, I.M. Ahmed, J.S. Alsharari, I.H. Alsohaimi, N.S. Al-Muaikel, T.S. Alraddadi, T.H. Hasanin, Adsorption of Cr (VI) using α-Fe2O3 coated hydroxy magnesium silicate (HMS): isotherm, thermodynamic and kinetic study, Int. J. Environ. Anal. Chem. 103 (10) (2023) 2223–2239, https://doi.org/10.1080/03067319.2021.1890061.

[51] H.M. Ali, A.A. Essawy, T.A.S. Elnasr, A.M. Aldawsari, I. Alsohaimi, H.M. Hassan, I.B. Abdel-Farid, Selective and efficient sequestration of Cr (VI) in ground water using trimethyloctadecylammonium bromide impregnated on Artemisia monosperma plant powder, J. Taiwan Inst. Chem. Eng. 125 (2021) 122–131, https://doi.org/10.1016/j.jtice.2021.05.051.

[52] I.H. Alsohaimi, M.S. Alhumaimess, M. Alzaid, A.A. Essawy, M.R. El-Aassar, R.M. Mohamed, H.M. Hassan, Tailoring confined CdS quantum dots in polysulfone membrane for efficiently durable performance in solar-driven wastewater remediating systems, J. Environ. Manag. 332 (2023) 117351, https://doi.org/10.1016/j.jenvman.2023.117351.

[53] M.S. Alamri, H.M. Hassan, M.S. Alhumaimess, A.M. Aldawsari, A.A. Alshahrani, T.S. Alraddadi, I.H. Alsohaimi, Kinetics and adsorption assessment of 1, 4-dioxane from aqueous solution by thiol and sulfonic acid functionalized titanosilicate, J. Mol. Liq. 362 (2022) 119786, https://doi.org/10.1016/j.molliq.2022.119786.

[54] I.H. Alsohaimi, M.S. Alhumaimess, A.A. Alqadami, H.M. Hassan, Q. Chen, M.S. Alamri, T.S. Alraddadi, Chitosan-carboxylic acid grafted multifunctional magnetic nanocomposite as a novel adsorbent for effective removal of methylene blue dye from aqueous environment, Chem. Eng. Sci. 280 (2023) 119017, https://doi.org/10.1016/j.ces.2023.119017.

[55] N.H. Solangi J. Kumar, S.A. Mazari, S. Ahmed, N. Fatima, N.M. Mubarak, Development of fruit waste derived bio-adsorbents for wastewater treatment: a review, J. Hazard Mater. 416 (2021) 125848, https://doi.org/10.1016/j.jhazmat.2021.125848.

[56] S. Nayar, A. Guha, Waste utilization for the controlled synthesis of nanosized hydroxyapatite, Mater. Sci. Eng. C 29 (4) (2009) 1326–1329, https://doi.org/10.1016/j.msec.2008.10.002.

[57] S. Pawar, T. Theodore, P.G. Hiremath, Synthesis of hydroxyapatite from avocado fruit peel and its application for hexavalent chromium removal from aqueous solutions-adsorption isotherms and kinetics study, Rasayan Journal of Chemistry 12 (4) (2019) 1964–1972, https://doi.org/10.31788/RJC.2019.1245425.

[58] I. Standard, Methods of sampling and test (physical and chemical) for water and wastewater, IS. Search in. IS3025 (Part 52) : 2003 (2006).

[59] H.M. Hassan, M.R. El-Aassar, M.A. El-Hashemy, M.A. Betiha, M. Alzaid, A. N Alqhobisi, I.H. Alsohaimi, Sulfanilic acid-functionalized magnetic GO as a robust adsorbent for the efficient adsorption of methylene blue from aqueous solution, J. Mol. Liq. 361 (2022) 119603, https://doi.org/10.1016/j.molliq.2022.119603.

[60] P.R. Choudhury, P. Mondal, S. Majumdar, Synthesis of bentonite clay based hydroxyapatite nanocomposites cross-linked by glutaraldehyde and optimization by response surface methodology for lead removal from aqueous solution, RSC advances 5 (122) (2015) 100838–100848, https://doi.org/10.1039/C5RA18490H.

[61] M.A. Shouman, N.A. Fathy, S.A. Khedr, A.A. Attia, Comparative biosorption studies of hexavalent chromium ion onto raw and modified palm branches, Advances in Physical Chemistry 1 (2013) 159712, https://doi.org/10.1155/2013/159712.

[62] Q. Fu, M.N. Rahaman, N. Zhou, W. Huang, D. Wang, L. Zhang, H. Li, In vitro study on different cell response to spherical hydroxyapatite nanoparticles, J. Biomater. Appl. 23 (1) (2008) 37–50, https://doi.org/10.1177/0885328207081350.

[63] S. Li, S. Hu, Y. Yan, Investigation of HAP nanoparticles absorbed by hepatoma cells in vitro, J. Wuhan Univ. Technol.-Materials Sci. Ed. 22 (2) (2007) 288–290, https://doi.org/10.1007/s11595-005-2288-3.

[64] M. Manoj, D. Mangalaraj, N. Ponpandian, C. Viswanathan, Core–shell hydroxyapatite/Mg nanostructures: surfactant free facile synthesis, characterization and their in vitro cell viability studies against leukaemia cancer cells (K562), RSC Adv. 5 (60) (2015) 48705–48711, https://doi.org/10.1039/C5RA04663G.

[65] Z. Yang, Y. Jiang, L. xin Yu, B. Wen, F. Li, S. Sun, T. Hou, Preparation and characterization of magnesium doped hydroxyapatite–gelatin nanocomposite, J. Mater. Chem. 15 (18) (2005) 1807–1811, https://doi.org/10.1039/B418015C.

[66] R. Mallampati, L. Xuanjun, A. Adin, S. Valiyaveettil, Fruit peels as efficient renewable adsorbents for removal of dissolved heavy metals and dyes from water, ACS Sustain. Chem. Eng. 3 (6) (2015) 1117–1124, https://doi.org/10.1021/acssuschemeng.5b00207.

[67] J. Dharmawan, S. Kasapis, P. Curran, Characterization of volatile compounds in selected citrus fruits from asia—Part II: peel oil, J. Essent. Oil Res. 20 (1) (2008) 21–24, https://doi.org/10.1080/10412905.2008.9699411.

[68] R. Foroutan, S.J. Peighambardoust, R. Mohammadi, S.H. Peighambardoust, B. Ramavandi, Application of walnut shell ash/ZnO/K2CO3 as a new composite catalyst for biodiesel generation from Moringa oleifera oil, Fuel 311 (2022) 122624, https://doi.org/10.1016/j.fuel.2021.122624.

[69] Z. Bonyadi P.S. Kumar, R. Foroutan, R. Kafaei, H. Arfaeinia, S. Farjadfard, et al., Ultrasonic-assisted synthesis of Populus alba activated carbon for water defluorination: application for real wastewater, Kor. J. Chem. Eng. 36 (10) (2019) 1595–1603, https://doi.org/10.1007/s11814-019-0373-0.

[70] R. Foroutan, S.J. Peighambardoust, S. Hemmati, H. Khatooni, B. Ramavandi, Preparation of clinoptilolite/starch/CoFe2O4 magnetic nanocomposite powder and its elimination properties for cationic dyes from water and wastewater, Int. J. Biol. Macromol. 189 (2021) 432–442, https://doi.org/10.1016/j.ijbiomac.2021.08.144.

[71] C. Zhang, X. Qin, Z. Xue, H. Shi, X. Meng, B. Feng, X. Wang, N. Yang, Water enhanced methanol decomposition for simultaneous heat recovery and ready-to-use synthesis gas production over CO2 capture enhanced Ni/zeolite 4A catalyst, Int. J. Hydrogen Energy 48 (57) (2023) 21701–21711, https://doi.org/10.1016/j.ijhydene.2023.03.065.

[72] K.T. Kubra, M.M. Hasan, M.N. Hasan, M.S. Salman, M.A. Khaleque, M.C. Sheikh, A.I. Rehan, A.I. Rasee, R.M. Waliullah, M.E. Awual, M.S. Hossain, A.K. D. Alsukaibi, H.M. Alshammari, M.R. Awual, The heavy lanthanide of Thulium (III) separation and recovery using specific ligand-based facial composite adsorbent, Colloids Surf. A Physicochem. Eng. Asp. 667 (2023) 131415, https://doi.org/10.1016/j.colsurfa.2023.131415.

[73] M. Foroughi, S.J. Peighambardoust, B. Ramavandi, R. Foroutan, N.S. Peighambardoust, Simultaneous degradation of methyl orange and indigo carmine dyes from an aqueous solution using nanostructured WO3 and CuO supported on Zeolite 4A, Sep. Purif. Technol. 344 (2024) 127265, https://doi.org/10.1016/j.seppur.2024.127265.

[74] B. Harikumar, M.K. Okla, S. Kokilavani, B. Almunqedhi, R. Alshuwaish, M.A. Abdel-Maksoud, S.S. Khan, Insights into oxygen defect enriched and non-metal dopant co modulated Fe3O4 nanospheres embedded WO3 nanorods for ameliorated photodegradation of doxycycline, Cr (VI) reduction and its genotoxicity, J. Clean. Prod. 398 (2023) 136549, https://doi.org/10.1016/j.jclepro.2023.136549.

[75] H.K. Yağmur, I. Kaya, Synthesis and characterization of magnetic ZnCl2-activated carbon produced from coconut shell for the adsorption of methylene blue, J. Mol. Struct. 1232 (2021) 130071, https://doi.org/10.1016/j.molstruc.2021.130071, 2021.

[76] A.A. Werkneh, N. Habtu, H.D. Beyene, Removal of hexavalent chromium from tannery wastewater using activated carbon primed from sugarcane bagasse: adsorption/desorption studies, Am. J. Appl. Chem. 2 (2014) 128–135, https://doi.org/10.11648/j.ajac.20140206.16.

[77] A.A. Attia, S.A. Khedr, S.A. Elkholy, Adsorption of chromium ion (VI) by acid activated carbon, Brazillian Journal of Chemical Engineering 27 (2010) 183–193, https://doi.org/10.1590/S0104-66322010000100016.

[78] P.S. Rao, S.R. Mise, G.S. Manjunatha, Kinetic studies on adsorption of chromium by coconut shell carbons from synthetic efuents, J Environ Sci Health Part A Environ Sci Eng Toxicol 27 (1992) 2227–2241, https://doi.org/10.1080/10934529209375851.

[79] R. Giri, N. Kumari, M. Behera, A. Sharma, S. Kumar, N. Kumar, R. Singh, Adsorption of hexavalent chromium from aqueous solution using pomegranate peel as low-cost biosorbent, Environmental Sustainability 4 (2) (2021) 401–417, https://doi.org/10.1007/s42398-021-00192-8.
[80] M. Aliabadi, I. Khazaei, H. Fakhraee, M.T.H. Mousavian, Hexavalent chromium removal from aqueous solutions by using low-cost biological wastes: equilibrium and kinetic studies, Int. J. Environ. Sci. Technol. 9 (2012) 319–326, https://doi.org/10.1007/s13762-012-0045-7.
[81] R. Pandey, N. Ansari, R. Prasad, M. Chavali, Pb(II) removal from aqueous solution by cucumissativus (cucumber) peel: kinetic, equilibrium & thermodynamic study, Am J Environ Prot 2 (2014) 51–58, https://doi.org/10.12691/env-2-3-1.
[82] M.K. Rai, G. Shahi, V. Meena, R. Meena, S. Chakraborty, R.S. Singh, B.N. Rai, Removal of hexavalent chromium Cr (VI) using activated carbon prepared from mango kernel activated with H3PO4, Resour Ef Technol 2 (2016) 63–70, https://doi.org/10.1016/j.reft.2016.11.01.
[83] T.S. Badessa, E. Wakuma, A.M. Yimer, Bio-sorption for efective removal of chromium(VI) from wastewater using Moringa stenopetala seed powder (MSSP) and banana peel powder (BPP), BMC Chem 14 (1) (2020) 1–12, https://doi.org/10.1186/s13065-020-00724-z.
[84] K.Y. Chena, J.C. Liub, P.N. Chiangc, S.L. Wanga, W.H. Kuand, Y.M. Tzoua, Y. Dengf, K.J. Tsenga, C.C. Chene, M.K. Wangg, Chromate removal as influenced by the structural changes of soil components upon carbonization at different temperatures, Environ. Pollut 162 (2012) 151–158, https://doi.org/10.1016/j.envpol.2011.10.036.
[85] H. Zhang, Y. Tang, D. Kai, X. Liu, X. Wang, Q. Huang, Z. Yu, Hexavalent chromium removal from aqueous solution by algal bloom residue derived activated carbon: equilibrium and kinetic studies, J. Hazard. Matter. 181 (2010) 801–808, https://doi.org/10.1016/j.envpol.2011.10.036.
[86] A.H. Jawad, A.M. Kadhum, Y.S. Ngoh, Applicability of dragon fruit (Hylocereus polyrhizus) peels as low-cost biosorbent for adsorption of methylene blue from aqueous solution: kinetics, equilibrium and thermodynamics studies, Desalin Water Treat 109 (2018) 231–240, https://doi.org/10.5004/dwt.2018.21976.
[87] S.H. Hasan, K.K. Singh, O. Prakash, M. Talat, Y.S. Ho, Removal of Cr (VI) from aqueous solutions using agricultural waste 'maize bran', J. Hazard Mater. 152 (1) (2008) 356–365, https://doi.org/10.1016/j.jhazmat.2007.07.006.
[88] D. Park, Y.S. Yun, J.H. Jo, J. Park, Efects of ionic strength, background electrolytes, heavy metals, and redox-active species on the reduction of hexavalent chromium by Ecklonia biomass, Journal of Microbiol Biotechnol 15 (2005) 780–786.
[89] Y. Ren, N. Yan, J. Feng, J. Ma, Q. Wen, N. Li, Q. Dong, Adsorption mechanism of copper and lead ions onto graphene nanosheet/δ-MnO2, Mater. Chem. Phys. 136 (2–3) (2012) 538–544, https://doi.org/10.1016/j.matchemphys.2012.07.023.
[90] R. Foroutan, R. Mohammadi, M. Taheri, A. Ahmadi, B. Ramavandi, Edible waste oil to biofuel using reclaimable g-C3N4/HAp/Fe3O4/K2CO3 nanobiocomposite catalyst: toxicity evaluation and optimization, Environ. Technol. Innov. 32 (2023) 103403, https://doi.org/10.1016/j.eti.2023.103403.
[91] R. Foroutan, S.J. Peighambardoust, R. Mohammadi, B. Ramavandi, D.C. Boffito, One-pot transesterification of non-edible Moringa oleifera oil over a MgO/K2CO3/HAp catalyst derived from poultry skeletal waste, Environ. Technol. Innov. 21 (2021) 101250, https://doi.org/10.1016/j.eti.2020.101250.
[92] R.L. Mason, R.F. Gunst, J.L. Hess, Statistical Design and Analysis of Experiments: with Applications to Engineering and Science, vol. 474, John Wiley & Sons, 2003.
[93] M. Dakiky, M. Khamis, A. Manassra, M. Mer'Eb, Selective adsorption of chromium (VI) in industrial wastewater using low-cost abundantly available adsorbents, Adv. Environ. Res. 6 (4) (2002) 533–540, https://doi.org/10.1016/S1093-0191(01)00079-X.
[94] R. Ansari, Z. Mosayebzadeh, Removal of basic dye methylene blue from aqueous solutions using sawdust and sawdust coated with polypyrrole, J. Iran. Chem. Soc. 7 (2) (2010) 339–350, https://doi.org/10.1007/BF03246019.
[95] N. Ali, A. Khan, S. Nawaz, M. Bilal, S. Malik, S. Badshah, H.M.N. Iqbal, Characterization and deployment of surface-engineered chitosan-triethylenetetramine nanocomposite hybrid nano-adsorbent for divalent cations decontamination, Int. J. Biol. Macromol. 152 (2020) 663–671, https://doi.org/10.1016/j.ijbiomac.2020.02.218.
[96] A. Khan, N. Ali, M. Bilal, S. Malik, S. Badshah, H.M.N. Iqbal, Engineering functionalized chitosan- based sorbent material: characterization and sorption of toxic elements, Appl. Sci. 9 (2019) 5138, https://doi.org/10.3390/app9235138.
[97] H. Freundlich, Über die adsorption in lösungen, Z. Phys. Chem. 57 (1) (1907) 385–470.
[98] A. Ali, M. Bilal, R. Khan, R. Farooq, M. Siddique, Ultrasound-assisted adsorption of phenol from aqueous solution by using spent black tea leaves, Environ. Sci. Pollut. Res. 25 (2018) 22920–22930, https://doi.org/10.1007/s11356-018-2186-9.
[99] Y.S. Ho, G. McKay, Pseudo-second order model for sorption processes, Process Biochem. 34 (5) (1999) 451–465.
[100] X. Yang, W. Zhu, Y. Song, H. Zhuang, H. Tang, Removal of cationic dye BR46 by biochar prepared from Chrysanthemum morifolium Ramat straw: a study on adsorption equilibrium, kinetics and isotherm, J. Mol. Liq. 340 (2021) 116617.
[101] R. Foroutan, S.J. Peighambardoust, S. Ghojavand, M. Foroughi, A. Ahmadi, F. Bahador, B. Ramavandi, Development of a magnetic orange seed/Fe3O4 composite for the removal of methylene blue and crystal violet from aqueous media, Biomass Conversion and Biorefinery (2023) 1–16.
[102] Y.-S. Ho, G. McKay, Pseudo-second order model for sorption processes, Process Biochem. 34 (5) (1999) 451–465.
[103] C. Aharoni, M. Ungarish, Kinetics of activated chemisorption. Part 1.—the non-elovichian part of the isotherm, journal of the chemical society, faraday transactions 1, Physical Chemistry in Condensed Phases 72 (1976) 400–408, https://doi.org/10.1039/F19767200400.
[104] E. Yakub, S.E. Agarry, F. Omoruwou, C.N. Owabor, Comparative study of the batch adsorption kinetics and mass transfer in phenol-sand and phenol-clay adsorption systems, Part. Sci. Technol. 1 (2019) 11, https://doi.org/10.1080/02726351.2019.1616862.
[105] Y. H Li, Z. Di, J. Ding, D. Wu, Z. Luan, Y. Zhu, Adsorption thermodynamic, kinetic and desorption studies of Pb2+ on carbon nanotubes, Water Res. 39 (2005) 605–609, https://doi.org/10.1016/j.watres.2004.11.004.
[106] A. Ashrafi, A. Rahbar-Kelishami, H. Shayesteh, Highly efficient simultaneous ultrasonic assisted adsorption of Pb (II) by Fe3O4@MnO2 core-shell magnetic nanoparticles: synthesis and characterization, kinetic, equilibrium, and thermodynamic studies, J. Mol. Struct. 1147 (2017) 40–47, https://doi.org/10.1016/j.molstruc.2017.06.083.
[107] L.G. Yan, Y.Y. Xu, H.Q. Yu, X.D. Xin, Q. Wei, B. Du, Adsorption of phosphate from aqueous solution by hydroxy-aluminum, hydroxy-iron and hydroxy-iron–aluminum pillared bentonites, J. Hazard Mater. 179 (2010) 244–250, https://doi.org/10.1016/j.jhazmat.2010.02.086.
[108] Y.J. Tu, C.F. You, Z. Zhang, Y. Duan, J. Fu, D. Xu, Strontium removal in seawater by means of composite magnetic nanoparticles derived from industrial sludge, Water 8 (8) (2016) 357, https://doi.org/10.3390/w8080357.
[109] X. Guo, A. Liu, J. Lu, X. Niu, M. Jiang, Y. Ma, M. Li, Adsorption mechanism of hexavalent chromium on biochar: kinetic, thermodynamic, and characterization studies, ACS Omega 5 (42) (2020) 27323–27331, https://doi.org/10.1021/acsomega.0c03652.